ELSEVIER

Journal of Nuclear Materials 305 (2002) 52–59

journal of nuclear materials

www.elsevier.com/locate/jnucmat

Microstructure of Ti5Al2.5Sn and Ti6Al4V deformed in tensile and fatigue tests

T. Leguey *, R. Schäublin, P. Marmy, M. Victoria

CRPP-EPFL Fusion Technology, Materials Group CH-5232 Villigen PSI, Switzerland

Received 5 December 2001; accepted 3 June 2002

Abstract

The microstructural characterization of two titanium alloys, Ti5Al2.5Sn and Ti6Al4V, was performed. These alloys were selected as representatives of the α and α + β titanium families, to investigate their possible application as structural materials in fusion reactor technology. Scanning and transmission electron microscopy have been used to obtain the relevant features of the microstructure in the as-received state and after mechanical deformation in tensile and fatigue experiments. Deformation modes and defects resulting from the deformation process were analyzed. Deformation occurred in the α phase of both alloys mainly through slip of the basal dislocations in basal, prismatic and pyramidal planes, together with slip in the $\langle c + a \rangle$ direction. A layered structure of dislocation loops developed in the α phase after cyclic fatigue tests. Deformation induced a phase transformation, namely a martensitic phase transition, that occurred solely in the β phase present in the Ti6Al4V alloy.

1. Introduction

Titanium alloys are being considered as structural materials for fusion reactor applications [1–3]. Among the reasons for their selection are the high strength-to-weight ratio, good mechanical and thermal properties and exceptional corrosion resistance. Moreover, they have low swelling tendency and fast induced radioactivity decay as compared with austenitic steels [4]. However, there are still some questions to be solved. The high affinity of titanium for hydrogen and its isotopes can lead to hydrogen embrittlement and a high tritium inventory [5,6]. For their use as first wall materials, the development of hydrogen barrier coatings will be a requirement to assure the maintenance of their mechanical properties as well as the safety conditions. The latest design of the next fusion reactor includes the use of titanium alloys in specific parts of the structure. In particular, the alloy Ti6Al4V has been proposed to be used in flexible supports between the ITER blanket modules and the vacuum vessel [7,8].

During the past a number of studies concerning radiation effects in titanium and titanium alloys has been carried out. Microstructural observations have focused mainly on alloys of the α + β family, where hcp (α) and bcc (β) phases coexist. In pure Ti, it has been observed that irradiation induces clusters of point defects in the form of dislocation loops [9]. In addition, it has been shown that ion irradiations at temperatures above 250 °C induce precipitations inside the α phase with a bcc structure [10–14]. The microstructure and mechanical properties have been also investigated in neutron [15–17] and proton [18] irradiated titanium alloys. Tensile tests at different temperatures show that α type alloys present better resistance to radiation embrittlement and less radiation hardening than α + β alloys. Microstructural observations again indicate β precipitation in the case of α + β or near-α alloys, while α ordered precipitates appear in the α alloys [16,17]. These different precipitation mechanisms have been proposed to be the reason of the

* Corresponding author. Permanent address: Deparmento de Física, Universidad Carlos III de Madrid, 28911 Leganés, Spain. Tel.: +34-91 6249413; fax: +34-91 6249430.

E-mail address: leguey@fis.uc3m.es (T. Leguey).

0022-3115/02/$ - see front matter
PII: S0022-3115(02)00888-7

observed changes in the mechanical properties caused by irradiation. This complex mechanism is not yet completely understood. Moreover, there is a lack of information on the interaction between radiation induced structural defects and radiation induced precipitates, and on their evolution during plastic deformation. In order to close this gap a complete understanding of the deformation induced microstructure of the unirradiated case is first needed.

In the present work two classical alloys, Ti5Al2.5Sn and Ti6Al4V, from the α and $\alpha+\beta$ families, respectively, are being investigated. The impact of proton irradiation on the tensile and fatigue properties of these alloys has been already described elsewhere [18]. In addition, tensile and fatigue experiments have been performed in both alloys in the unirradiated state for a wide range of temperatures [19]. The tensile strength of both alloys is comparable to that found for ferritic/martensitic steels. The uniform elongation of the $\alpha+\beta$ alloy is slightly lower than in the α alloy. In the fatigue experiments both alloys show different behaviour for low and high imposed strain regimes. At high imposed strains there is constant softening, though contrary to the low imposed strain regime that induces significant softening followed by hardening to the end of life.

We present a detailed study of the microstructure of the two alloys in the unirradiated state before and after the deformation tests. Deformation mechanisms and microstructural changes in relation with the mechanical properties are discussed.

2. Experimental

The two titanium alloys investigated were the α alloy Ti5Al2.5Sn, and the $\alpha+\beta$ alloy Ti6Al4V. Bars of 32 mm in diameter of Ti5Al2.5Sn (specification AMS 4926H) were provided by Howmet Mill, USA. After hot forming they were annealed for 1 h at 815 °C and then air cooled. Ti6Al4V was provided by Timet SA, France, in the shape of 150 mm diameter bars (DIN 65040). After hot forming in the $\alpha+\beta$ field the material was annealed at 730 °C for 1.5 h and subsequently air cooled. Chemical analyses of both alloys are presented in Table 1.

Non-standard microtensile flat specimens were prepared according to PIREX specifications [20]. Thickness and gauge length are 0.34 and 5.5 mm, respectively. Uniaxial tensile tests were performed in a RMC100 testing machine. The tests were realized between room temperature and 475 °C in vacuum of about 10^{-3} mbar for high-temperature tests. Samples were deformed up to fracture at constant strain rate of 3×10^{-4} s^{-1}.

Cylindrical tubular specimens with internal diameter of 2.7 mm, thickness of 0.35 mm and a gauge length of 5.5 mm were used for the fatigue tests. The tests were performed in the same RMC100 machine at constant temperature of 350 °C in vacuum and under total strain control ($R=-1$). The strain rate varied between 0.001 and 0.002 s^{-1} (6–12%/min).

SEM and TEM examinations were made on the as-received alloys and on selected specimens after the completion of the deformation tests. Three millimetre disks were cut next to the fracture surface and mechanically polished to reduce the thickness up to $\simeq$100 μm. SEM was performed with a Philips XLF-30 microscope. Thin foils for TEM were prepared by electropolishing using a solution of 3% perchloric acid, 37% 2-butoxyethanol and 60% ethanol at 20 V and −35 °C. The TEM thin foils were examined with a JEOL 2010 microscope operated at 200 kV. Both microscopes were equipped with energy dispersive X-ray spectrometers (EDS) for microanalysis. The defects associated with the deformation were imaged using the bright/dark field and weak beam techniques. It appears that the best diffraction conditions to analyze dislocations in the hcp phase are found close to the zone axis $[2\bar{1}\bar{1}0]$. There, the diffraction vectors (0002), $(01\bar{1}0)$ and $(01\bar{1}1)$ allow to identify the Burgers vectors $1/3\langle11\bar{2}0\rangle$ (characteristic of $\langle a\rangle$-type dislocations), and $\langle0001\rangle$ (corresponding to $\langle c\rangle$-type dislocations). The best diffraction vector in terms of image quality is $(01\bar{1}1)$.

3. Results and discussion

3.1. Microstructure of the as-received alloys

Fig. 1 shows SEM micrographs of both alloys. The initial microstructure of Ti5Al2.5Sn consisted in equiaxed α grains, 15–40 μm in size. Element contrast obtained by BSE and EDS showed that there is about 1% of the retained second phase, which is rich in iron. The distribution of this phase is anisotropic, with a preferential orientation along the rod axis (see Fig. 1(a) and

Table 1
Chemical composition of the alloys (wt%)

Alloy	Al	V	Sn	Fe	C	H_2	N_2	O_2	Ti
Ti5Al2.5Sn	5.0	–	2.4	0.36	0.17	0.036	0.010	0.179	balanced
Ti6Al4V	6.08	3.95	–	0.14	0.0056	<0.006	0.0065	0.176	balanced

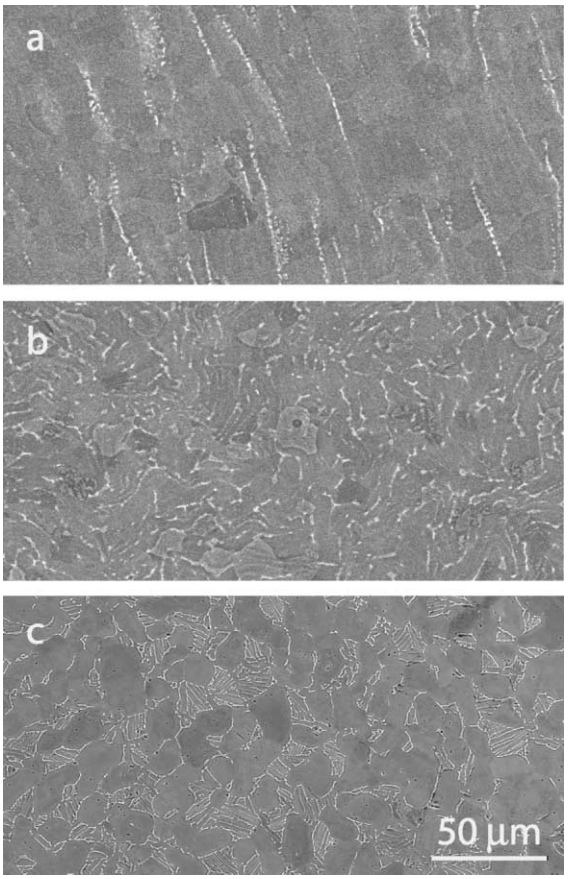

Fig. 1. Backscattered SEM micrographs of as-received titanium alloys: (a) Ti5Al2.5Sn, longitudinal section; (b) Ti5Al2.5Sn, transversal section; (c) Ti6Al4V, transversal section.

(b)). Specimens for the deformation test were cut in the longitudinal direction to minimize the effect of this texture.

Ti6Al4V has a duplex structure, as can be seen in Fig. 1(c). It is composed of equiaxed primary α grains of about 20 μm size, together with colonies of elongated secondary α grains, of approximately 1 μm width and 10–15 μm length. They are surrounded by the intergranular β phase. The total content of β phase was estimated to be about 13% in volume.

Fig. 2 shows the main characteristics of the as-received Ti5Al2.5Sn alloy as seen by TEM. Despite the annealing the microstructure is not completely recovered and features related to the rolling process can still be observed within the grains. Fig. 2(a) shows irregular arrays of dislocations. They are inhomogeneously distributed throughout all the grains. Dislocation analysis revealed that the majority are basal dislocations with the $\langle a \rangle$ Burgers vector $(1/3\langle 2\bar{1}\bar{1}0\rangle)$. Isolated dislocations with the $\langle c+a \rangle$ Burgers vector $(1/3\langle 11\bar{2}3\rangle)$ could also be observed, mainly near the grain boundaries. There are also some traces of deformation bands, parallel to the basal planes, probably generated during the rolling process (see Fig. 2(b)). Characterization of the second phase detected was performed by electron diffraction and EDS measurements. The crystalline structure was determined as bcc (Fig. 2(c)). Chemical microanalyses showed that all the iron present in the alloy was confined to this phase, for it could not be detected in the hcp matrix. This result is in agreement with previous studies showing the importance of iron impurities as β stabilizers [21]. The remaining β phase was not only intergranular, but was also found inside the α grains, appearing as big precipitates with sizes up to 1 μm.

TEM pictures of as-received Ti6Al4V are shown in Fig. 3. As mentioned above the primary α grains are not completely recovered, showing sometimes a parallel subgrain structure (Fig. 3(a)), with laths of about 300 nm width. Small arrays of short dislocations can be seen within these subgrains (Fig. 3(b)). Tilting experiments confirmed that they are $\langle a \rangle$-type dislocations. Fig. 3(c) shows a general view of the secondary α grains and the intergranular β phase. Misorientation between the different α laths from the same colony was not larger than 2–3°, and their orientation with respect to the β phase follows the Burgers relation [22]:

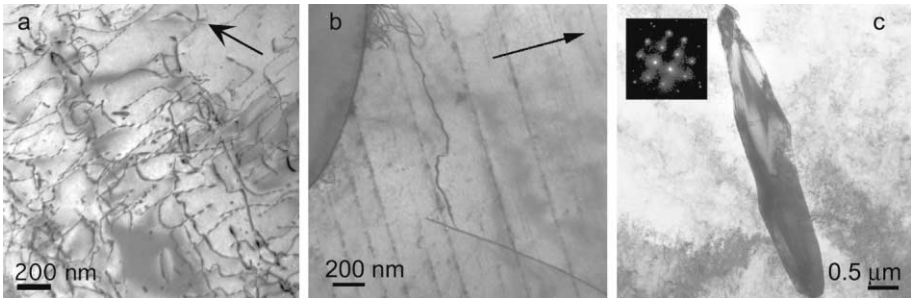

Fig. 2. TEM pictures of as-received Ti5Al2.5Sn: (a) *a*-type dislocations array, $\vec{g} = (1\bar{1}0\bar{1})[10\bar{1}1]$; (b) *c*-component dislocations and basal slip bands, $\vec{g} = (0002)[10\bar{1}0]$; (c) residual β phase, Z.A. = $[100]$. The arrow denotes the $\vec{g}$ vector employed for the 2-beam condition.

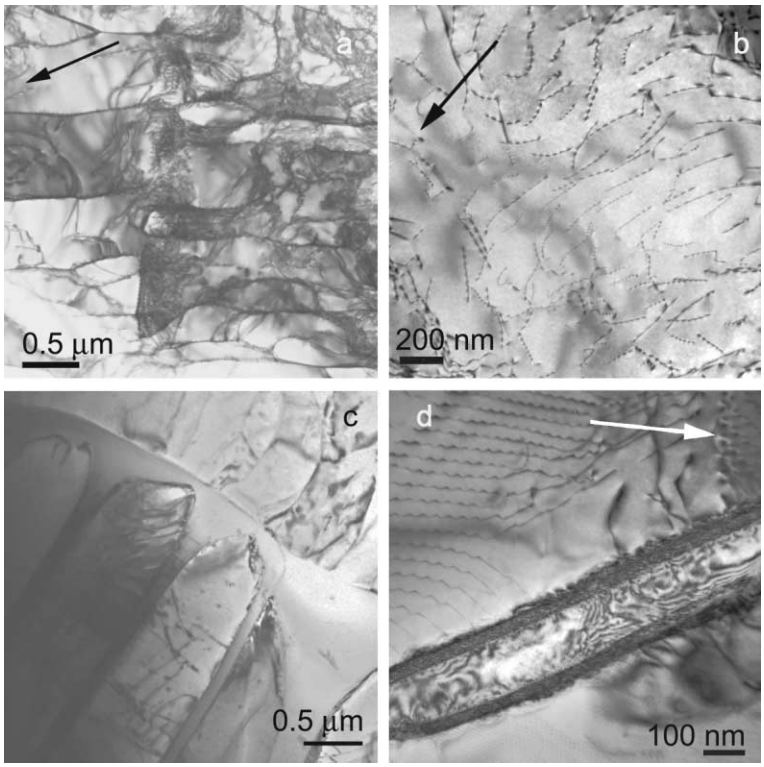

Fig. 3. TEM pictures of as-received Ti6Al4V: (a) subgrain structure in the primary α grains, $\vec{g} = (0\bar{1}\,1\,1)[7\bar{2}\bar{5}3]$; (b) *a*-type dislocations array, $\vec{g} = (0\bar{1}\,1\,1)[2\bar{1}\bar{1}0]$; (c) secondary α grains and intergranular β phase; (d) interfacial phase between α and β grains, $\vec{g} = (1\bar{1}0\bar{1})[2\bar{1}\bar{1}3]$. The arrow denotes the $\vec{g}$ vector employed for the 2-beam condition.

$$\{1\,1\,0\}_{\beta}||\{0\,0\,0\,1\}_{\alpha}, \quad \langle 1\,1\,1\rangle_{\beta}||\langle 1\,1\,\bar{2}\,0\rangle_{\alpha}$$

indicating their origin as transformed products from previous β grains when the temperature was above the β transition temperature. Inhomogeneous dislocation arrays were also observed both in the secondary α grains and in the remaining β phase.

Another different phase was also detected in the interfaces between the α and β grains (see Fig. 3(d)). This phase appears to be a Ti hydride, as the diffraction pattern showed. As the samples were prepared by the electropolishing technique it is reasonable to consider this phase as an artifact due to the intake of hydrogen during the thinning process [23].

3.2. Microstructure after tensile tests

Fig. 4 shows TEM examples of the main features observed in the Ti5Al2.5Sn alloy after mechanical tensile testing up to fracture. Samples tested at RT and at 350 °C showed no significant differences in the resulting microstructure. The samples exhibit long parallel deformation bands and subgrains. Also, a cellular dislocation structure can be seen near the grain boundaries (see Fig. 4(a) and (b)). A high density of long parallel dislocations was observed (Fig. 4(b)). They are homogeneously distributed throughout all the grains and they are much longer than the ones observed in the as-received specimens. Tilt experiments showed that they are $\langle a\rangle$-type basal dislocations. Fig. 4(b) shows the crossing of two of these families of basal dislocations with deformation bands. Fig. 4(c) shows a detail of the intersection area, where isolated dislocation loops resulting from the interaction of the different families of basal dislocations can be distinguished. The appearance of these loops will be discussed more in detail in Section 3.3. Main gliding planes were determined as prismatic and pyramidal planes. Grains with different orientations also activate preferential slip on basal planes. These three slip modes are $\{1\,0\bar{1}\,0\}\langle 1\,2\bar{1}\,0\rangle$, $\{0\,0\,0\,1\}\langle 1\,2\bar{1}\,0\rangle$ and $\{1\,0\bar{1}\,1\}\langle 1\,2\bar{1}\,0\rangle$. The majority of the dislocations analyzed have a nearly pure screw character. No twins were detected. In some grains, shorter arrays of dislocations with $\langle c + a\rangle$ component are seen (Fig. 4(d)), but they are not as frequent as the basal ones. These $\langle c + a\rangle$ dislocations can constitute a slip mode allowing elongation along the *c* axis, and in this situation twinning would be not the necessary mechanism for a general deformation, as it is the case for pure titanium [24].

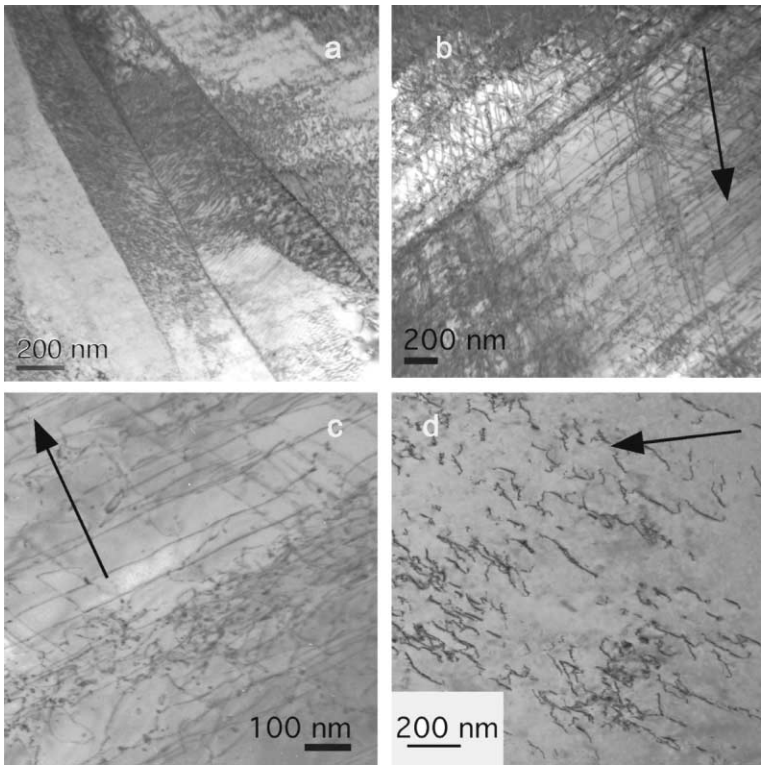

Fig. 4. TEM micrographs of deformed Ti5Al2.5Sn tensile tested: (a) deformation subgrains; (b) slip bands and *a*-type dislocation array, $\vec{g} = (0\bar{1}10)[0001]$; (c) intersection of *a*-type dislocation arrays, $\vec{g} = (0\bar{1}11)[2\bar{1}\bar{1}3]$; (d) $\langle c + a \rangle$ dislocation array, $\vec{g} = (0002)[2\bar{1}\bar{1}0]$. The arrow denotes the $\vec{g}$ vector employed for the 2-beam condition.

The microstucture of the tensile-tested Ti6Al4V alloy specimens are quite similar to the Ti5Al2.5Sn alloy for the primary α grains. See for instance Fig. 5(a), where deformation induced subgrains can be seen, and Fig. 5(b), where again high density of long parallel $\langle a \rangle$-type dislocations are present. Fig. 5(c) shows the structure resulting in the larger β regions, the zones comprised between a primary α grain and two secondary α laths. After the deformation, they have developed a lamellar structure with parallel needles of 30–50 nm thickness. Electron diffraction patterns were used to elucidate whether they are twins or a different phase. It appears that their crystalline structure is hcp, which corresponds in this situation to the α′ martensite. It is known that martensitic transformations occur in α and α + β titanium alloys during quenching from the high temperature β phase, where either a hexagonal (α′) or an orthorhombic (α″) martensite appears [25]. The martensitic transformation from the metastable β phase can also be triggered by an external stress [26], as it has been ob-

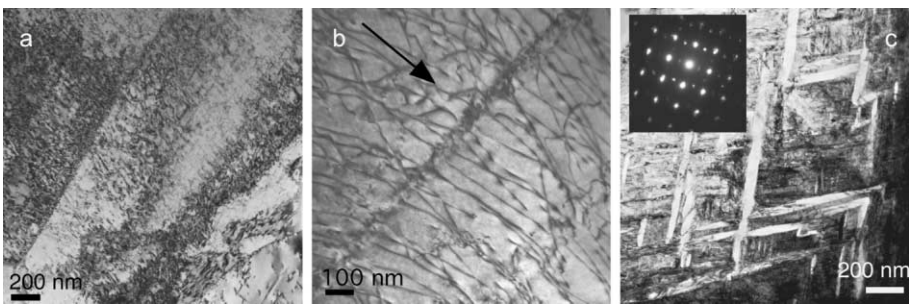

Fig. 5. TEM pictures of deformed Ti6Al4V tensile tested: (a) deformation subgrains; (b) slip bands and *a*-type dislocation array, $\vec{g} = (0\bar{1}11)[2\bar{1}\bar{1}3]$; (c) deformation induced martensite in β grain. The arrow denotes the $\vec{g}$ vector employed for the 2-beam condition.

served in our case. It also agrees with the observations made in the β grains after the fatigue tests, where the amount of the transformed phase is much higher.

3.3. Microstructure after fatigue tests

The characteristic microstructure found in the samples tested in fatigue can be observed in Figs. 6 and 7. The same behavior was found in the α grains of both alloys. There, the iterative extension–compression cycles of the fatigue process induce a large damage. α grains appear divided by subgrain boundaries with a high density of entangled dislocations and small defects in the subgrains (see Fig. 6(a)). As in the samples deformed in tension, the majority of the dislocations present are of the *a*-type. Although single dislocations cannot be readily seen, slip planes are apparent. Fig. 6(b) shows basal slip bands in a single grain, while Fig. 6(c) shows the bands that are produced in common prismatic planes of contiguous grains. These results are consistent with the preferential slip systems found previously. Moreover, the simultaneous activation of both systems, prismatic and basal, in the same grain has also been observed [27]. In addition, small defects appear to be grouped in a layered structure that follows the prismatic slip planes. These bands have an approximate thickness of $\lesssim 100$ nm, which is wider than the one found for basal slip bands. Fig. 6(d) shows a weak beam image, where these layers are seen, separated by nearly defect-free regions. It should be noted that the imaging condition used here, $\vec{g} = (10\bar{1}0)$, would render 2/3 of *a*-type defects visible. This proves their absence in the depleted areas. The existence of such defect-free areas between defect planes suggests that the strain is strongly localized during the fatigue process. The defects present in these prismatic planes show a disordered structure. Short dislocations can be found, together with a high density of small dislocation loops and fragments (see Fig. 7(a) and (b)). Tilting experiments showed that most of them are pure *a*-type defects. Some small scale features show residual contrast under invisibility imaging conditions for basal dislocations (see Fig. 6(b)). These contrast features are attributed to dislocation loops. Tilting experiments using the inner–outer contrast of loops were performed and both interstitial and vacancy loops were characterized. The size of the loops is quite variable, ranging from 2 to 12 nm. Dislocation loops can arise from the repeated mutual interactions of *a*-type dislocations, as previously observed in the case of the microstructure induced by tensile test (Fig. 4(c)). The high density of dislocation

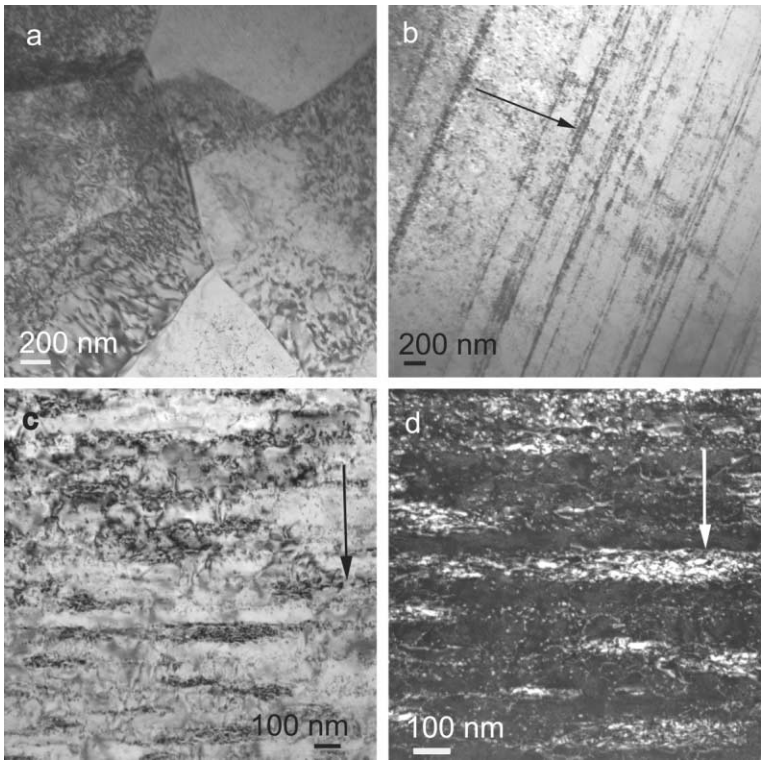

Fig. 6. TEM pictures of deformed Ti5Al2.5Sn tested in fatigue: (a) deformation induced subgrains; (b) basal slip bands, $\vec{g} = (0002)[10\bar{1}0]$; (c) prismatic slip bands, $\vec{g} = (10\bar{1}0)[0001]$; (d) same as (c), weak beam g(5g). The arrow denotes the $\vec{g}$ vector employed for the 2-beam condition.

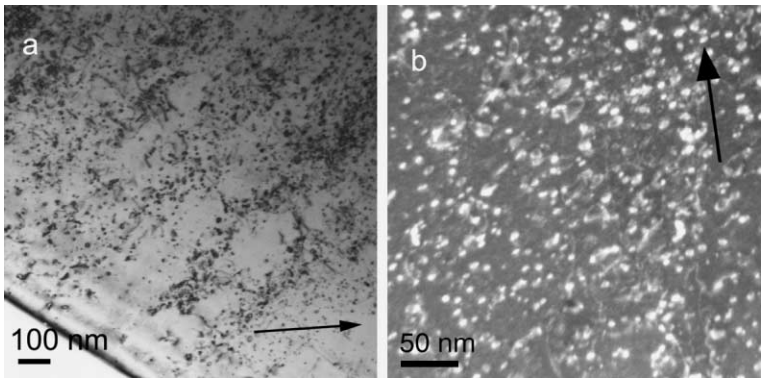

Fig. 7. TEM pictures of deformed Ti6Al4V tested in fatigue: (a) dislocation loops and debris, $\vec{g} = (0\bar{1}11)[7\bar{2}\bar{5}3]$; (b) same as (a), weak beam g(4g). The arrow denotes the $\vec{g}$ vector employed for the 2-beam condition.

loops and dipoles after prismatic slip appears to be a common characteristic of hcp metals. It was suggested that the intersection of screw dislocations with a $1/3\langle 11\bar{2}0\rangle$ Burgers vector will produce jogs in dislocation gliding in non-basal planes, while they will not be so formed when they are gliding in the basal planes [28]. This indicates that cross slip is a necessary condition for the dislocation loop structure to occur.

4. Conclusions

The two alloys Ti5Al2.5Sn and Ti6Al4V show similar characteristics in the uniaxial deformation process for the α phase; basal dislocations are dominant, gliding in prismatic, pyramidal and basal planes, depending on the orientation with respect to the tensile axis. Slip of $\langle c + a\rangle$ dislocations is also activated, and twinning is not observed, in contrast to pure titanium. A martensitic phase transformation is induced by straining in the β phase of the Ti6Al4V alloy. Cyclic fatigue tests develop a layered structure of dislocation loops in the prismatic planes.

Acknowledgements

The present work was partially financed by the European Fusion Technology Materials Program. The European Commission is acknowledged by its support through the Marie Curie Fellowship Programme. We also thank the Paul Scherrer Institute (Villigen, CH) for the overall use of the facilities.

References

[1] J. Davis, M.A. Ulrichson, R.A. Causey, J. Nucl. Mater. 212–215 (1994) 813.
[2] B. van der Schaaf, K. Ehrlich, P. Fenici, A.A. Tavassoli, M. Victoria, Fusion Eng. Des. 48 (2000) 499.
[3] G. Kalinin, V. Barabash, A. Cardella, J. Dietz, K. Ioki, R. Matera, R. Santoro, R. Tivey, T.I.H. Teams, J. Nucl. Mater. 283–287 (2000) 10.
[4] A. Kumar, H.W. Kugel, G. Ascione, Fusion Eng. Des. 42 (1998) 329.
[5] S. Kelzenberg, E. Ehrlich, J. Nucl. Mater. 226 (1995) 319.
[6] R.H. Jones, H.L. Heinisch, K.A. McCarthy, J. Nucl. Mater. 271&272 (1999) 518.
[7] K. Ioki, V. Barabash, A. Cardella, F. Elio, Y. Gobar, G. Janeschitz, G. Johnson, G. Kalinin, D. Lousteau, M. Onozuka, R. Parker, G. Sannazzaro, R. Tivey, J. Nucl. Mater. 258–263 (1998) 74.
[8] K. Ioki, V. Barabash, A. Cardella, F. Elio, H. Iida, G. Johnson, G. Kalinin, N. Miki, M. Onozuka, G. Sannazzaro, Y.U.M. Yamada, Fusion Eng. Des. 49&50 (2000) 467.
[9] T. Leguey, N. Baluc, R. Schäublin, M. Victoria, 'Structure/mechanics relationships in proton irradiated pure titanium', presented at 10th Int. Conf. on Fusion Reactor Materials, Baden. Baden, Germany, Oct. 2001, J. Nucl. Mater. (2002).
[10] P. Wilkers, G.L. Kulcinski, J. Nucl. Mater. 78 (1978) 427.
[11] R.H. Jones, L.A. Charlot, J. Nucl. Mater. 91 (1980) 329.
[12] G. Ayrault, J. Nucl. Mater. 113 (1983) 1.
[13] D.L. Plumton, G.L. Kulcinski, R.A. Dodd, J. Nucl. Mater. 144 (1987) 252.
[14] D.L. Plumton, G.L. Kulcinski, R.A. Dodd, J. Nucl. Mater. 144 (1987) 264.
[15] D.R. Duncan, R.J. Puigh, E.K. Opperman, J. Nucl. Mater. 103&104 (1981) 919.
[16] Y. Higashiguchi, H. Kayano, M. Miyake, J. Nucl. Mater. 103&104 (1981) 925.
[17] O.A. Kozhevnikov, E.V. Nesterova, V.V. Rybin, I.I. Yarmolovich, J. Nucl. Mater. 271&272 (1999) 472.
[18] P. Marmy, T. Leguey, J. Nucl. Mater. 296 (2001) 155.
[19] P. Marmy, T. Leguey, I. Belianov, M. Victoria, J. Nucl. Mater. 283–287 (2000) 602.
[20] P. Marmy, R. Yuzhen, M. Victoria, J. Nucl. Mater. 179–181 (1991) 697.

[21] W.F. Smith, Structure and Properties of Engineering Alloys, McGraw-Hill Series in Materials Science and Engineering, McGraw-Hill, New York, 1993.
[22] W.G. Burgers, Physica 1 (1934) 561.
[23] D. Banerjee, C.G. Shelton, B. Ralph, J.C. Williams, Acta Metall. 36 (1988) 125.
[24] T. Leguey, C. Bailat, N. Baluc, M. Victoria, MRS Symp. Proc. 650 (2001) R.3.1.1.
[25] R. Boyer, et al. (Eds.), Materials Properties Handbook: Titanium Alloys, ASM International, Materials Park, OH, 1994.
[26] M. Niinomi, T. Kobayashi, I. Inagaki, A.W. Thompson, Met. Trans. A 21 (1990) 1733.
[27] G. Baxter, W.M. Rainforth, L. Grabowski, Acta Metall. 44 (1996) 3453.
[28] P.G. Partridge, Metall. Rev. 118 (1967) 169.